

In situ metrology to characterize water vapor delivery during atomic layer deposition

Tariq Ahmido, William A. Kimes, Brent A. Sperling, Joseph T. Hodges, and James E. Maslar

Citation: *Journal of Vacuum Science & Technology A* **34**, 031512 (2016); doi: 10.1116/1.4948360

View online: <http://dx.doi.org/10.1116/1.4948360>

View Table of Contents: <http://scitation.aip.org/content/avs/journal/jvsta/34/3?ver=pdfcov>

Published by the AVS: Science & Technology of Materials, Interfaces, and Processing

Articles you may be interested in

Atomic layer deposition of molybdenum oxide using bis(tert-butylimido)bis(dimethylamido) molybdenum

J. Vac. Sci. Technol. A **32**, 01A119 (2014); 10.1116/1.4843595

Critical tensile strain and water vapor transmission rate for nanolaminate films grown using Al₂O₃ atomic layer deposition and alucone molecular layer deposition

Appl. Phys. Lett. **101**, 234103 (2012); 10.1063/1.4766731

In situ diagnostics for studying gas-surface reactions during thermal and plasma-assisted atomic layer deposition

J. Vac. Sci. Technol. A **30**, 01A158 (2012); 10.1116/1.3670404

In situ synchrotron based x-ray fluorescence and scattering measurements during atomic layer deposition: Initial growth of HfO₂ on Si and Ge substrates

Appl. Phys. Lett. **98**, 231905 (2011); 10.1063/1.3598433

Improved electrical properties of Pt / HfO₂ / Ge using in situ water vapor treatment and atomic layer deposition

Appl. Phys. Lett. **98**, 102905 (2011); 10.1063/1.3562015



Instruments for Advanced Science

 <p>Gas Analysis</p> <ul style="list-style-type: none">dynamic measurement of reaction gas streamscatalysis and thermal analysismolecular beam studiesdissolved species probesfermentation, environmental and ecological studies	 <p>Surface Science</p> <ul style="list-style-type: none">UHV TPDSIMSend point detection in ion beam etchelemental imaging - surface mapping	 <p>Plasma Diagnostics</p> <ul style="list-style-type: none">plasma source characterizationetch and deposition process reactionkinetic studiesanalysis of neutral and radical species	 <p>Vacuum Analysis</p> <ul style="list-style-type: none">partial pressure measurement and control of process gasesreactive sputter process controlvacuum diagnosticsvacuum coating process monitoring
--	---	---	---

Contact Hiden Analytical for further details:
W www.HidenAnalytical.com
E info@hiden.co.uk
CLICK TO VIEW our product catalogue

In situ metrology to characterize water vapor delivery during atomic layer deposition

Tariq Ahmido,^{a)} William A. Kimes, Brent A. Sperling, Joseph T. Hodges, and James E. Maslar

Material Measurement Laboratory, National Institute of Standards and Technology, 100 Bureau Drive, Stop 8320, Gaithersburg, Maryland 20899-8320

(Received 19 February 2016; accepted 18 April 2016; published 2 May 2016)

Water is often employed as the oxygen source in metal oxide atomic layer deposition (ALD) processes. It has been reported that variations in the amount of water delivered during metal oxide ALD can impact the oxide film properties. Hence, one contribution to optimizing metal oxide ALD processes would be to identify methods to better control water dose. The development of rapid, quantitative techniques for *in situ* water vapor measurements during ALD processes would be beneficial to achieve this goal. In this report, the performance of an *in situ* tunable diode laser absorption spectroscopy (TDLAS) scheme for performing rapid, quantitative water partial pressure measurements in a representative quarter-inch ALD delivery line is described. This implementation of TDLAS, which utilizes a near-infrared distributed-feedback diode laser and wavelength modulation spectroscopy, provides measurements of water partial pressure on a timescale comparable to or shorter than the timescale of the gas dynamics in typical ALD systems. Depending on the degree of signal averaging, this TDLAS system was capable of measuring the water partial pressure with a detection limit in the range of ~ 0.80 to ~ 0.08 Pa. The utility of this TDLAS scheme was demonstrated by using it to identify characteristics of a representative water delivery system that otherwise would have been difficult to predict. Those characteristics include (1) the magnitude and time dependence of the pressure transient that can occur during water injection, and (2) the dependence of the steady-state water partial pressure on the carrier gas flow rate and the setting of the water ampoule flow restriction. [<http://dx.doi.org/10.1116/1.4948360>]

I. INTRODUCTION

Atomic layer deposition (ALD) is a deposition technique that is widely employed for depositing nanometer-scale, conformal layers of metal oxides, e.g., high permittivity (high ϵ) gate dielectrics in complementary metal oxide semiconductor technology and capacitor dielectrics in dynamic random access memory technology.¹⁻⁴ For deposition of metal oxides, water is often employed as the oxygen source.¹⁻⁴ It has been shown that varying the amount of water utilized during metal oxide ALD can result in differences in the deposition rate,^{5,6} oxide phase or structure,⁷⁻¹⁰ and electrical properties^{5,10} of the deposited film. Hence, to minimize variations in film properties, it is important to reproducibly deliver water during ALD processes, preferably in known quantities. The development of rapid, quantitative techniques for *in situ* water vapor measurements during ALD processes would help achieve this goal, whether such a technique was utilized as an in-line process diagnostic or an off-line metrology for evaluating different water delivery systems.

A number of analytical techniques have been used to measure the partial pressure of water vapor in semiconductor process gases, including optical spectroscopy, mass spectrometry, quartz crystal microbalance, chilled mirror hygrometer, and capacitance-based sensor techniques.¹¹ A measurement technique in ALD processes must be compatible with systems operating at low pressures (ALD processes generally operate at pressures between 13 and 1333 Pa)^{3,4}

and elevated temperatures, while providing rapid response and having a minimal impact on the design of the deposition system. Such requirements have resulted in relatively few techniques being utilized for time-resolved water vapor measurements during ALD processes. Reported investigations in this area have utilized either Fourier transform infrared (FT-IR) spectroscopy¹² or tunable diode laser absorption spectroscopy (TDLAS).¹³⁻¹⁵ While the FT-IR spectroscopy-based investigation described by Sperling *et al.*¹² provided quantitative water measurements, the temporal resolution of FT-IR spectroscopy is generally insufficient to capture the water partial pressure transients which may be present in an ALD injection cycle.

TDLAS methods can potentially provide higher temporal resolution than FT-IR spectroscopy, making such techniques better suited for ALD process measurements. Inman *et al.*¹³ utilized a TDLAS system based on a mid-IR lead salt diode laser and employing wavelength modulation spectroscopy (WMS) to monitor water vapor in an ALD system using the water transition at 1456.888 cm^{-1} . While monitoring water transitions in the mid-IR compared to the near-IR spectral region offers the potential for lower detection limits (the line strength of water transitions in the mid-IR can be significantly larger than transitions in the near-IR), near-IR lasers tend to be less expensive than mid-IR lasers and can be easier to integrate into an optical system (near-IR lasers packaged with silica fiber optic coupling are widely available). Hence, if sensitivity in the near-IR is not a limitation, there are advantages to employing near-IR TDLAS. Previous

^{a)}Electronic mail: tariq.ahmido@nist.gov

reports have described monitoring water vapor during ALD processes using near-IR TDLAS with WMS (Ref. 14) and without WMS.¹⁵ However, these reports described neither the quantitative measurement of water partial pressure (i.e., no effort was made to calibrate the relationship between optical response and water partial pressure) nor the overall performance of the near-IR TDLAS water measurement system (no description of detection limit or noise characteristics was provided). Hence, it is difficult to quantitatively evaluate the potential of near-IR TDLAS measurements for in-line water delivery measurements based on previous reports.

There are two main objectives of this report: (1) to describe the performance of a near-IR TDLAS technique for rapid, quantitative measurements of water partial pressure during water injection in an ALD delivery line and (2) to demonstrate the utility of this technique by identifying performance characteristics of a representative ALD water delivery system that otherwise would be difficult to predict.

II. EXPERIMENTAL DETAILS

A. TDLAS system

Figure 1 shows a schematic of the *in situ* optical system used for TDLAS measurements. A near-IR distributed-feedback diode laser was used to probe the rovibrational water transition $(\nu_1, \nu_2, \nu_3)_{J_{Ka,Kc}} = (0,0,0)_{3_{0,3}} \rightarrow (1,0,1)_{2_{0,2}}$ at 7181.156 cm^{-1} . At room temperature, this transition has a line intensity of $1.51 \times 10^{-20} \text{ cm molecule}^{-1}$.¹⁶ For quantitative measurements, the pressure in the optical cell was kept below 1333 Pa, which ensured that the water transition line was primarily Doppler-broadened and isolated from other water lines. The peak absorption cross section was $4.8 \times 10^{-19} \text{ cm}^2 \text{ molecule}^{-1}$ at room temperature. Wavelength selection was achieved by using a commercially available temperature controller, which regulated the temperature of the laser head to $\pm 10^{-3} \text{ K}$. To obtain a better signal-to-

noise ratio than generally possible with direct absorption techniques, a WMS scheme was employed in which the optical signal detected at the second harmonic of the modulation frequency (the 2f signal) is theoretically proportional to the water vapor partial pressure in the beam path.¹⁷⁻¹⁹ Wavelength modulation was achieved by using a function generator to modulate the laser current from a commercially available current source ($\pm 0.01 \text{ mA}$ current resolution). The laser wavelength was modulated across the 7181.156 cm^{-1} transition at 30 kHz and at a frequency modulation depth of approximately 0.02 cm^{-1} , the nominal full-width at half-maximum (FWHM) of the Doppler-broadened water line. A wavelength meter was used to verify that the laser wavelength tuning range corresponded to the water transition. The laser output was coupled into a single-mode fiber, which was subsequently split in a 90:10 ratio. The output of each leg was collimated. The higher-power leg was directed through the optical flow cell, and the lower-power leg was directed to a reference cell containing pure water vapor. Each leg was monitored using nominally identical 10 MHz-bandwidth InGaAs photodetectors with integrated preamps and electronic band-pass filters. The 2f signal that was in-phase with the laser modulation frequency was monitored using a lock-in amplifier with a 3 ms integration time. Upon start-up of the laser diode (the laser was not typically operated overnight), it was verified that the laser emission wavelength coincided with the water absorption line wavelength by observing the reference cell detector signal on an oscilloscope as the laser wavelength was scanned across the water transition wavelength (as a result of the current modulation) and adjusting the DC current on the laser current driver as necessary. The nominally constant 2f reference detector signal was also used to optimize experimental parameters prior to *in situ* flow measurements in the delivery line in the following manner. First, the DC current on the laser current driver was adjusted to produce the maximum 2f reference signal

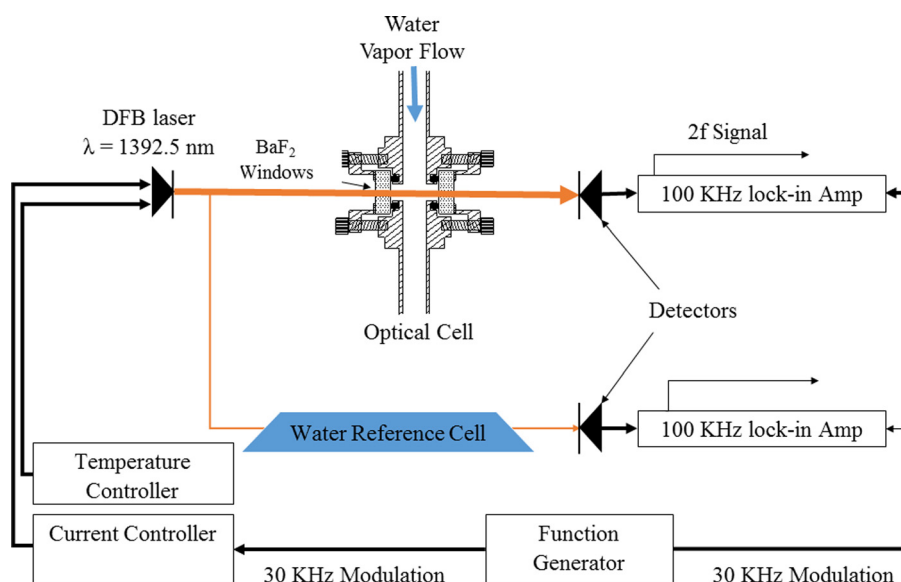


FIG. 1. (Color online) Schematic of the *in situ* optical system used for the TDLAS measurements.

(while the oscilloscope was monitored to ensure that the modulated laser wavelength was still scanning across the water transition). Then, the lock-in amplifier phase was adjusted to produce the maximum $2f$ reference signal. The DC current and lock-in amplifier phase were further adjusted in an iterative process. The reference detector was only used for these functions and prior to flow measurements; all subsequent $2f$ signal measurements described in this report only refer to the $2f$ signal from the flow cell detector. The flow cell detector $2f$ signal was digitized at a rate of 300 or 100 Hz.

The in-line optical flow cell was designed to simulate the flow conditions in a delivery line by boring a 4.8 mm diameter hole (the nominal internal diameter of quarter inch tubing used to construct the water delivery system) into a stainless steel block. Optical access was achieved by mounting two uncoated BaF₂ windows (12.7 mm diameter \times 2 mm thick with a 0.5° wedge to reduce étaloning effects) on opposite sides of the steel block, the window-to-block seals being made with elastomer O-rings. Measurements were made in a single-pass and the optical path length from window surface to window surface inside the cell was 5 mm. The optical cell was maintained at nominally 110 °C for all measurements described in this report, with heating accomplished by jacketing the cell with aluminum blocks into which cartridge heaters were inserted. The optical path in the laboratory ambient was enclosed with lens tubes to minimize laser intensity fluctuations on the detector when the optical cell was heated.²⁰

The reference cell was a glass tube with Brewster-angle windows at each end and a path length of about 45 cm. The reference cell was at ambient temperature and contained about 266 Pa of water vapor.

B. Water delivery system

Figure 2 shows a schematic of the water delivery system. It was designed to minimize water pressure transients in the delivery line to a deposition chamber and has been used to deposit ALD metal oxides for a number of investigations.²¹ The design is a variation on typical water delivery systems that employ a needle valve to control water flow rate,²² and the rationale for the variation will be discussed in more detail subsequently. The geometry of the delivery system was based on commercially available quarter-inch (outside diameter) tubing commonly used in ALD injection systems. The flow lines were electropolished stainless steel tubes with a 4.8 mm internal diameter and a 6.3 mm outer diameter (quarter inch tubing). The carrier gas was 99.999% nitrogen and the flow rate was controlled by a thermal mass flow controller (MFC). Water vapor was delivered from a nominally 0.5 L stainless steel ampoule containing deionized water with a resistivity of 18 M Ω cm or greater at 21 °C. No active temperature control was employed for the water ampoule (the ampoule was exposed to the laboratory ambient). Water flow rates were controlled using a manual needle valve as a variable flow orifice. The needle valve was a bellows-sealed metering valve with a micrometer handle which permitted the valve stem position to be measured in 0.0254 mm increments. One complete turn of the valve nominally corresponded to a 0.635 mm valve stem movement. Water was introduced into the carrier gas via a fast-switching, pneumatically actuated three-port injection valve located on the delivery line. The water reservoir line was vented to a dry scroll pump using an additional fast-switching, pneumatically actuated three-port vent valve. The three-port valves employed in this work were configured in a “T” in which the

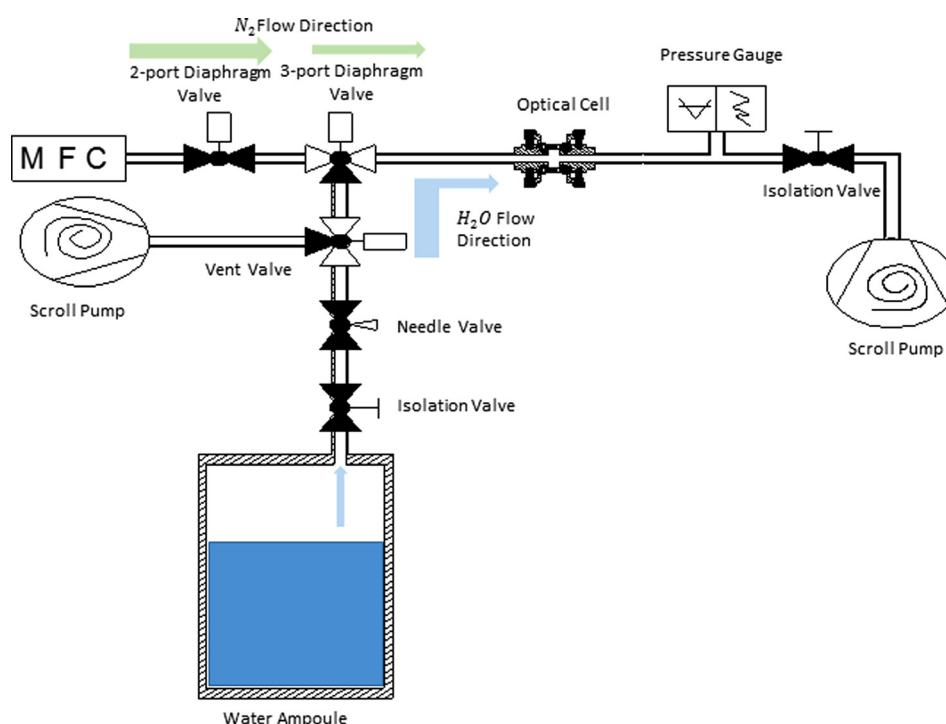


FIG. 2. (Color online) Schematic of the water delivery system.

stem of the T was valved and flow was unimpeded through the arm of the T (see Fig. 2 for a representation).

Venting the water reservoir line is the previously mentioned variation on the typical water delivery system. While water delivery systems such as that described in Ref. 22 are straightforward to assemble and provide adjustable water flow rates (if not always a well quantified water flow rate), these systems can exhibit initial pressure transients during water injection. This is because, even when water is not being injected into the delivery line, water can diffuse into the volume between the injection valve and the needle valve (this volume is subsequently referred to as V_{i-n}); given time, the water vapor partial pressure in V_{i-n} will increase to the vapor pressure of water at the temperature of V_{i-n} . When the injection valve is opened, a positive pressure transient will occur. The configuration employed for this work allows V_{i-n} to be vented and thereby control the degree to which V_{i-n} pressurizes between water injections. In other words, the water flow can be established through the venting valve before switching the water flow to the delivery line, thereby decreasing pressure transients.

Optical access to the water delivery line was achieved via the installation of the optical flow cell. The total system pressure was measured approximately 12.5 cm downstream of the optical flow cell using a capacitance diaphragm gauge (CDG) that was temperature-controlled at 100 °C and that had a 1.33×10^3 Pa (10 Torr) full scale range. The nominal carrier gas molar flow rates at standard temperature and pressure (0 °C and 101.3 kPa) ranged from 75 ml/min (standard cm^3 per min, subsequently denoted as SCCM) to 150 ml/min (SCCM) and the corresponding nominal total pressure ranged from 600 to 910 Pa at the pressure gauge location. The lines and valves from the pneumatically actuated two-port valve and the needle valve to the pressure gauge (see Fig. 2) were heated using a series of heating tapes. The analog output of the CDG was digitized at the same rate as the TDLAS 2f signal.

For water delivery measurements, water was introduced into the carrier gas stream in the following manner. First, the MFC was set to the desired flow rate and the pneumatically actuated two-port valve was opened to initiate gas flow. Second, the needle valve was set to the position needed to control the ultimate water flow rate. Third, the vent valve was opened to vent water vapor from V_{i-n} . Fourth, the vent valve was closed. Fifth, the injection valve was opened after a time delay (t_{delay}). Sixth, the injection valve was closed after the desired injection time.

III. CHARACTERIZING THE TDLAS SYSTEM PERFORMANCE

Figure 3 shows (a) the measured signal and corresponding water vapor partial pressure during a single water injection compared to the signal averaged for 100 injections and (b) the standard deviation of the background and signal for a single injection and from 2 to 100 averaged injections. For each injection, the standard deviation of the background and the signal was obtained for the time interval of 0.5–1.5 s and

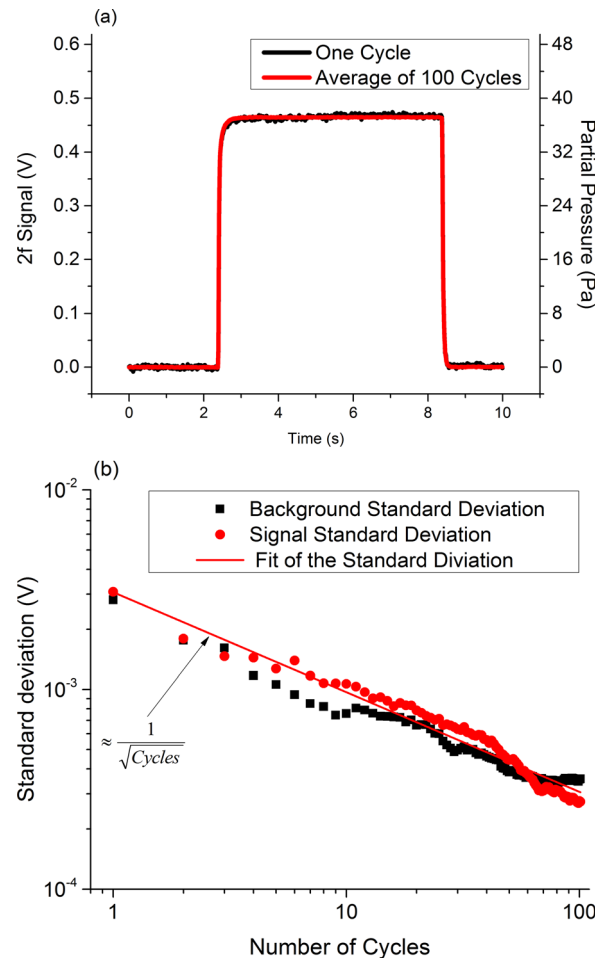


Fig. 3. (Color online) (a) Measured signal and corresponding water vapor partial pressure during a single water injection compared to the signal for 100 averaged injections and (b) standard deviation of the background and signal for a single injection and from 2 to 100 averaged injections. The solid line has a slope equal to the square root of the reciprocal of the number of injection cycles.

5.0–7.0 s, respectively. Figure 3(b) shows that the signal-to-noise ratio can be readily improved by averaging multiple injections up to at least 100 injections.

The optical response of the measurement system was calibrated by measuring the 2f signal as a function of pure static water pressure in the optical cell, i.e., in the absence of a carrier gas and with no gas flow. Static conditions were achieved by closing the up-stream two-port pneumatic valve and the down-stream isolation valve (see Fig. 2) and then directly injecting different amounts of water vapor without a carrier gas. The background 2f signal and pressure transducer voltage were measured when the system was pumped down to the scroll pump base pressure and the respective background measurements were subtracted from the 2f signal and pressure transducer signal measured during water injection. Figure 4 shows a typical set of 2f signal values and corresponding water vapor density values (calculated from the measured water pressure assuming ideal gas behavior). The 2f signal and water density values shown in Fig. 4 were obtained from the average of forty water injections. The system sensitivity, S , corresponds to the slope of a proportional

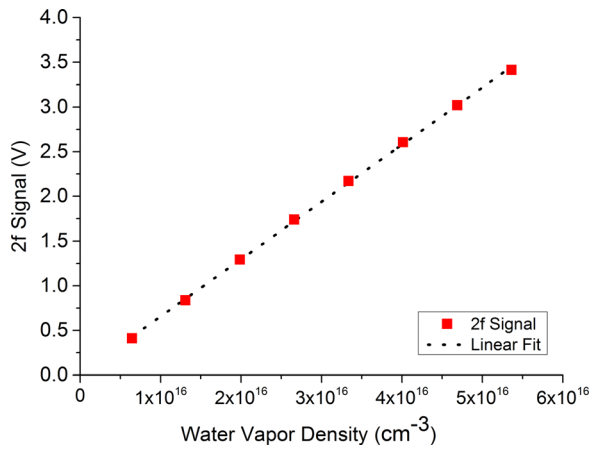


FIG. 4. (Color online) Example of the proportional relationship between the 2f signal and water vapor density.

fit to the relationship shown in Fig. 4. For this example, $S = 6.41 \times 10^{-17} \text{ V cm}^{-3}$.

The detection limit, q_L , of this technique can be estimated using the following:²³

$$q_L = \frac{k s_{bl}}{S}, \quad (1)$$

where the constant k is a numerical factor corresponding to the desired confidence level and s_{bl} is the standard deviation of the blank measurements. From Fig. 3(b), the s_{bl} value ranges from approximately 3×10^{-3} for a single injection to 3×10^{-4} for the average of 100 injections in this typical example. The corresponding range of q_L is from $1.40 \times 10^{14} \text{ cm}^{-3}$ ($\sim 0.80 \text{ Pa}$ water partial pressure) to $1.40 \times 10^{13} \text{ cm}^{-3}$ ($\sim 0.08 \text{ Pa}$ water partial pressure) for values of $S = 6.41 \times 10^{-17} \text{ V cm}^{-3}$ and $k = 3$.

In order to characterize the stability of the optical system, S values obtained over a period of two weeks were compared. The value of S tended to vary $<2\%$ over a day, but could vary by as much as 9% from day to day. The reason for the variation is unknown. However, it is presumably related to drifts in the laser wavelength or output intensity, caused by, for example, changes in the laboratory ambient temperature. This presumption is supported by the observation that changes in S value were reasonably correlated with changes in the laser output power (data not shown).

IV. CHARACTERIZING THE WATER DELIVERY SYSTEM PERFORMANCE

In this section, the utility of TDLAS system is demonstrated by identifying performance characteristics of the ALD water delivery system described previously (see Sec. II B) with an emphasis on characteristics that would be difficult to identify without a technique such as TDLAS. The emphasis is not on the measured values of water partial pressure because these values will strongly depend on the specifics of the deposition system (e.g., the vacuum conductance and measurement geometry), making it difficult to use the data measured here to estimate the performance of a different delivery system.

As discussed previously, a concern for some water delivery systems is the presence of a pressure transient prior to establishing steady-state flow conditions. Such a transient can negatively impact a deposition process, especially one involving short water injection times. In the present water delivery system configuration, pressure transients can be observed depending on the length of t_{delay} (the time delay between closing the vent valve and opening the injection valve). This is illustrated in Fig. 5, which shows the time-dependent (a) water partial pressure and (b) total pressure for t_{delay} values equal to 0.70, 0.38, and 0.10 s. Water was injected as previously described (see Sec. II B). The total water injection time was 6 s, the carrier gas flow rate was 75 ml/min (SCCM), and the needle valve position was one turn open. For $t_{\text{delay}} = 0.70 \text{ s}$ (the longest delay), positive water pressure transients were observed at the optical cell and pressure transducer. These positive transients are attributed to a water pressure in V_{i-n} that was significantly higher than the carrier gas pressure in the delivery line.

The magnitude of the water partial pressure transient measured with the TDLAS is about $8.5\times$ greater than that measured with the CDG. The duration of the transient

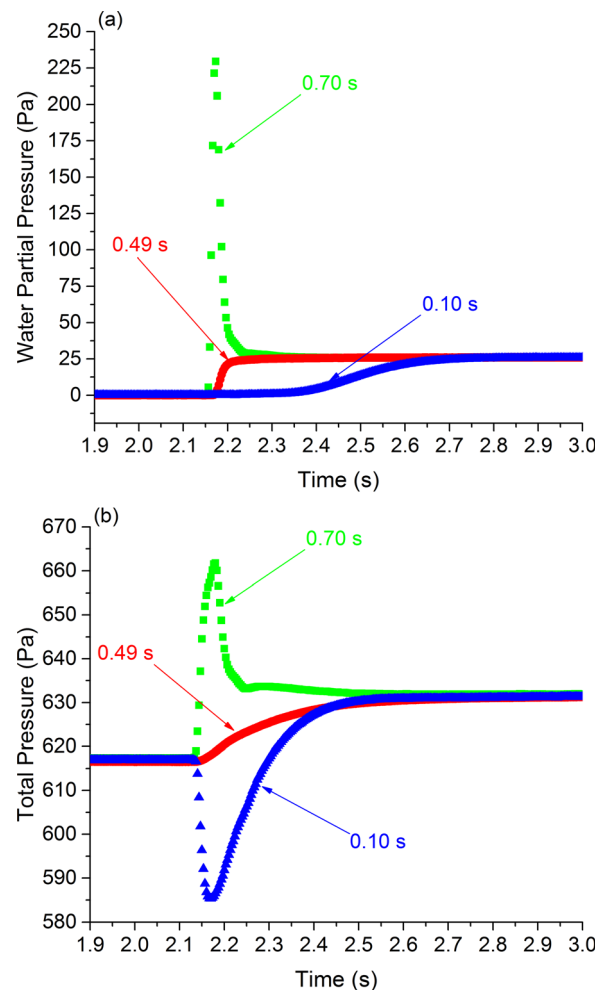


FIG. 5. (Color online) Time-dependent (a) water partial pressure and (b) total pressure for t_{delay} values equal to 0.70, 0.49, and 0.10 s. The carrier gas flow rate was 75 ml/min (SCCM) and the needle valve position was one turn open.

(FWHM) measured with the TDLAS is about $2.5\times$ narrower than that measured with the CDG. These differences are attributed to the slower response time of the CDG, which the manufacturer specifies as 30 ms.

For $t_{\text{delay}} = 0.10$ s (the shortest delay), the observation of the initial water signal and the establishment of the steady-state water signal are both delayed compared to the other two t_{delay} values. In addition, a negative pressure transient is observed at the pressure transducer. These characteristics are attributed to a water pressure in V_{i-n} that was lower than the carrier gas pressure in the delivery line, causing carrier gas to flow from the delivery line into V_{i-n} prior to the establishment of steady-state flow. For $t_{\text{delay}} = 0.38$ s (the intermediate delay time), the time-dependent water partial pressure profile corresponds fairly closely to that observed for $t_{\text{delay}} = 0.70$ s (i.e., only a small delay in the observation of the initial water signal and the establishment of steady-state flow) but without the positive pressure transient. In the case of the total pressure, no transients are observed either.

If one had no means to measure the water partial pressure, one could try to estimate it from the difference between the total pressure with only nitrogen flowing and with nitrogen and water flowing. However, this method can be flawed, as illustrated in Fig. 5(a). For $t_{\text{delay}} = 0.38$ s, the water partial pressure measured using TDLAS was 25.6 Pa, while the total pressure increased by only $632.0 - 617.4$ Pa = 14.6 Pa. This difference indicates that adding the water flow caused the nitrogen partial pressure to decrease. That decrease likely occurred because the flow through the isolation valve (see Fig. 2) was viscous or transitional, not molecular, and increasing the total pressure increased the flow conductance of the valve (decreasing the nitrogen partial pressure corresponding to a given nitrogen flow rate).

For the current and related water delivery systems, the needle valve position ultimately controls the water flux from the water reservoir. However, the relationship between the needle valve position and the water partial pressure in the delivery line is not necessarily simple. Figure 6 shows the steady-state water partial pressure as a function of (a) needle valve position for a series of carrier gas flow rates and (b) flow rate for a series of needle valve positions. As expected, the water partial pressure increases with increasing needle valve position [see Fig. 6(a)]. However, the relationship between water partial pressure and needle valve position is not expressed by a single function. At intermediate valve positions (two to five turns open), the relationship is approximately linear with a slope that depends on the flow rate, while at other positions the relationships are nonlinear.

In contrast to the influence of needle valve position, an increase in carrier gas flow rate results in a decrease in water partial pressure at a given needle valve position [see Fig. 6(b)]. The decrease in water partial pressure could be attributed to at least two effects, depending on the pressure drop across the injection valve. If the pressure in the delivery line is less than approximately half of the pressure upstream of the injection valve, then flow through the injection valve is choked and the water flow rate through this valve is independent of the delivery line pressure. In this case, the

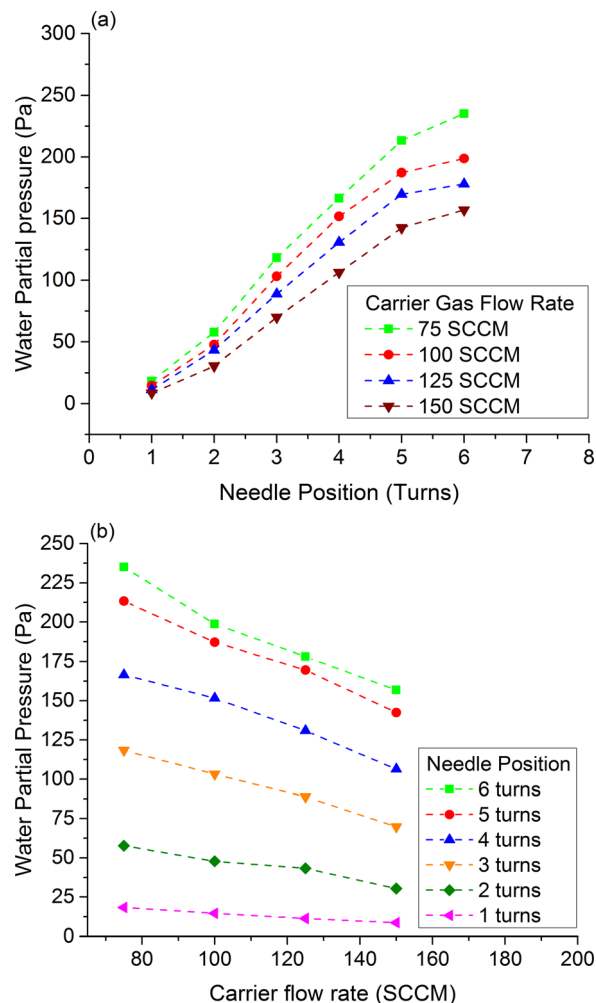


Fig. 6. (Color online) Steady-state nominal water partial pressure as a function of (a) needle valve position for a series of carrier gas flow rates and (b) flow rate for a series of needle valve positions. (The dashed lines are shown as an aid to the eye.)

observed decrease in water partial pressure with increasing carrier gas flow rate (and delivery line pressure) is attributed to the increased conductance of the isolation valve at higher pressures. If the pressure in the delivery line is greater than approximately half of the pressure upstream of the injection valve, then flow through the injection valve is not choked and the water flow rate through this valve is dependent of the delivery line pressure. In this case, the observed decrease in water partial pressure with increasing carrier gas flow rate is attributed also to a decreased pressure drop across the injection valve and a concomitant decrease in water flow rate across the valve and into the delivery line. In either case, the dependence of water partial pressure in the delivery line with carrier gas flow would have been difficult to predict without a measurement technique such as TDLAS.

V. CONCLUSION

The performance of a near-infrared TDLAS scheme for *in situ*, rapid, quantitative measurements of water partial pressure in a representative quarter-inch ALD delivery line was demonstrated, with minimal impact on the geometry of

the line and, hence, flow dynamics in the line. Depending on the degree of signal averaging, the TDLAS system was capable of measuring the water partial pressure with a detection limit in the range of 0.80–0.08 Pa (at $k=3$) at a maximum sampling rate of 300 Hz. The utility of this TDLAS scheme was demonstrated on a representative water delivery system by identifying performance characteristics that would be difficult to identify without such a measurement technique. Water partial pressure transients were readily measured, allowing valve actuation times to be optimized to minimize those transients. The dependence of water partial pressure on both needle valve position and on carrier gas flow rate was also established, each exhibiting a dependence that otherwise would have been difficult to predict.

- ¹V. Miiikkulainen, M. Leskela, M. Ritala, and R. L. Puurunen, *J. Appl. Phys.* **113**, 021301 (2013).
- ²K. Kukli, M. Heikkila, M. Ritala, and M. Leskela, *Adv. Eng. Mater.* **11**, 223 (2009).
- ³M. Ritala and J. Niinisto, *Chemical Vapour Deposition: Precursors, Processes and Applications*, edited by A. C. Jones and M. L. Hitchman (Royal Society of Chemistry, Cambridge, 2009), pp. 158–206.
- ⁴M. Schumacher, P. K. Baumann, and T. Seidel, *Chem. Vap. Deposition* **12**, 99 (2006).
- ⁵R. Kuse, M. Kundu, T. Yasuda, N. Miyata, and A. Toriumi, *J. Appl. Phys.* **94**, 6411 (2003).
- ⁶R. Matero, A. Rahtu, M. Ritala, M. Leskela, and T. Sajavaara, *Thin Solid Films* **368**, 1 (2000).
- ⁷J. Aarik, A. Aidla, H. Mandar, T. Uustare, K. Kukli, and M. Schuisky, *Appl. Surf. Sci.* **173**, 15 (2001).
- ⁸J. Aarik, A. Aidla, V. Sammelselg, H. Siimon, and T. Uustare, *J. Cryst. Growth* **169**, 496 (1996).
- ⁹J. Aarik, A. Aidla, V. Sammelselg, and T. Uustare, *J. Cryst. Growth* **181**, 259 (1997).
- ¹⁰K. Kukli *et al.*, *J. Appl. Phys.* **96**, 5298 (2004).
- ¹¹H. H. Funke, B. L. Grissom, C. E. McGrew, and M. W. Raynor, *Rev. Sci. Instrum.* **74**, 3909 (2003).
- ¹²B. A. Sperling, W. A. Kimes, J. E. Maslar, and P. M. Chu, *J. Vac. Sci. Technol., A* **28**, 613 (2010).
- ¹³R. Inman, A. Deshpande, D. Chraibi, and G. Jursich, paper presented at the SEMI Technology Symposium: Innovations in Semiconductor Manufacturing, San Jose, CA, 2003.
- ¹⁴J. E. Maslar, W. S. Hurst, D. R. Burgess, W. A. Kimes, N. V. Nguyen, E. F. Moore, and J. T. Hodges, *ECS Trans.* **13**, 139 (2008).
- ¹⁵M. Pemble, I. M. Povey, and F. Chalvet, *ECS Trans.* **11**, 155 (2007).
- ¹⁶R. A. Toth, *Appl. Opt.* **33**, 4851 (1994).
- ¹⁷J. Reid and D. Labrie, *Appl. Phys. B* **26**, 203 (1981).
- ¹⁸W. H. Weber *et al.*, *Appl. Spectrosc.* **56**, 706 (2002).
- ¹⁹J. A. Silver, *Appl. Opt.* **31**, 707 (1992).
- ²⁰W. A. Kimes, E. F. Moore, and J. E. Maslar, *Rev. Sci. Instrum.* **83**, 083106 (2012).
- ²¹J. Maslar, J. Hoang, W. A. Kimes, and B. A. Sperling, *Appl. Spectrosc.* **69**, 54A (2015).
- ²²J. W. Elam, M. D. Groner, and S. M. George, *Rev. Sci. Instrum.* **73**, 2981 (2002).
- ²³IUPAC, *Pure Appl. Chem.* **45**, 99 (1976).